

Growth of carbon and nitrogen containing precipitates in crystalline solar silicon and their influence on solar cells

Susanne Richter¹, Jan Bauer², and Otwin Breitenstein^{*,2}

¹ Fraunhofer Center for Silicon Photovoltaics CSP, Otto-Eißfeldt-Str. 12, 06120 Halle (Salle), Germany

² Max Planck Institute of Microstructure Physics, Weinberg 2, 06120 Halle (Saale), Germany

Received 20 October 2016, revised 19 January 2017, accepted 19 January 2017

Published online 2 February 2017

Keywords multicrystalline silicon, silicon carbide, silicon nitride, precipitates, solar cells

* Corresponding author: e-mail breiten@mpi-halle.mpg.de, Phone: +49 345 5582 740, Fax: +49 345 5511 223

The growth mechanisms, structural, mechanical, and electrical properties of silicon carbide and silicon nitride precipitates in solar silicon are reviewed and some new aspects about the distribution of trace elements in these precipitates are reported in this review. SiC and Si₃N₄ precipitates may have detrimental impact on the quality of solar silicon material. Therefore intensive research has been done at these precipitates in the past, which is summarized first. The properties

of the different types of precipitates reported in literature are then described in detail. Especially SiC precipitates may have detrimental impact on the electrical behavior of solar cells by causing severe ohmic shunting. Furthermore SiC precipitates are very hard and may harm the wafering process. An outlook of the impact of such precipitates on new cell concepts and new solar silicon materials, such as n-type, is given.

© 2017 WILEY-VCH Verlag GmbH & Co. KGaA, Weinheim

1 Introduction About 93% of the global photovoltaic production in 2015 was provided by crystalline silicon technology wherein 69% are represented by multicrystalline silicon (mc-Si) [1]. Most mc-Si ingots are grown by the Bridgman or vertical gradient freeze (VGF) process where usually a silica (quartz) crucible with an amorphous silicon nitride coating is applied [2]. Today's mc-Si module efficiencies range around 18%, compared to monocrystalline silicon (mono-Si) modules which achieve >20%. The difference in module efficiencies has to be explained by the differences between mono- und multicrystalline silicon material properties as structure and purity. These properties resulting from the different manufacturing processes are responsible for defect formation. Beside crystallographic structural defects in mc-Si ingots as grain boundaries and dislocations also precipitates of compounds of Si with impurity atoms can occur diminishing the quality of the material [3]. It has to be distinguished between

metallic precipitates, which are mostly of microscopic size as, for example, FeSi₂ precipitates, which are responsible for breakdown effects in mc-Si solar cells as reported in [4, 5], and non-metallic precipitates, whose size ranges from some μm to some mm. Within this article the formation of the non-metallic carbon and nitrogen correlated precipitates [3, 6, 7] as well as their physical properties within p-type silicon are in focus. Effects on solar cell parameters and therefore the efficiency are discussed as well as mechanical properties and possible techniques to avoid such precipitates. SiC precipitates, for instance, may alter the electric behavior by providing shunt paths in solar cells. Furthermore they influence the sawing process due to their hardness and may therefore be detrimental to the production yield of solar wafers. Until today silicon manufacturers have to deal with SiC and Si₃N₄ precipitates [8]. This review is intended to give an overview about the research on SiC and Si₃N₄ precipitates in the last decades in Sec-

tion 2. Detailed results about their growth, their structural (morphology, crystallography), electrical, and mechanical properties are given in Section 3. In the course of the presentation of the results in Section 3 already the effects of the precipitates on the material, the solar cells, and on processes are discussed. In Section 4 a more general discussion is given about the role of these precipitates in new cell concepts and in n-type material. Strategies about their avoidance are discussed to give an impression of the role of SiC and Si₃N₄ precipitates in the future of photovoltaic energy conversion.



Susanne Richter studied physics at the University of Leipzig and wrote her diploma thesis in the field of solid state physics. Since 2008 she is working at the Fraunhofer Center for Silicon Photovoltaics CSP in the group of Diagnostics of Solar Cells. In 2015 she received her Ph.D. in physics on the topic of elemental and structural analysis of precipitates

in multicrystalline silicon at the Martin Luther University Halle-Wittenberg. Her daily scientific business deals with microstructural diagnostics and chemical analysis of photovoltaic materials. In 2016, she was awarded for her work with a young academics prize of the Heinz-Bethge Foundation for Applied Electron Microscopy.



Jan Bauer received the Diploma degree in physics from the University of Halle-Wittenberg, Germany in 2006, for investigating shunting precipitates in Si solar cell materials, and the Ph.D. degree in solar cell characterization, particular under reverse bias, in 2009 from University of Halle-Wittenberg, in cooperation with the Max Planck Institute of Microstructure

Physics, Halle, Germany. After being researcher with Calisolar Inc., Berlin (Germany)/Sunnyvale (CA, USA), he is now a postdoc with the Max Planck Institute of Microstructure Physics.



Otwin Breitenstein received his Ph.D. in physics at the University of Leipzig, Germany, in 1980. Since 1992 he is with Max Planck Institute of Microstructure Physics in Halle, Germany, where he investigates defects in semiconductors. Since 1999 he is using lock-in thermography for detecting internal shunts in silicon solar cells. Since 2001 he has introduced this technique on a microscopic scale for isolating faults in ICs. As an associate professor at Halle University he has given lectures on the physics of solar cells and on advanced characterization techniques. He is author of a book on Lock-in Thermography and has published more than 200 contributions about his research in scientific journals and at international conferences.

2 Historical overview – A coarse chronology of research on SiC and Si₃N₄ precipitates in mc-Si materials

In the year 1953 the first $2 \times 2 \text{ cm}^2$ sized monocrystalline silicon solar cells were developed by Chapin, Fuller, and Pearson at Bell Laboratories in New Jersey, USA [9]. The efficiency was up to 6%, and since then a lot has happened in material improvement and physical understanding. From the beginning of solar cell development in science and industry, material quality was a major focus in research. Multicrystalline silicon material started to edge into the market and accompanies the monocrystalline because of its lower price in the 1990s [10]. Beside the challenge to avoid structural defects in the material, such as dislocations and their recombination activity due to metallic impurities (especially in mc-Si), contamination with non-metallic impurities plays an important role as well. Due to their affinity to build stable, mesoscopic crystals with silicon, carbon and nitrogen have important impact on the material properties. SiC precipitates in Si solar cells (in this case in edge-defined film-fed grown (EFG) ribbon solar cells) have been found already in 1976 [11]. The sources of carbon detected in the Si material were found to stem from graphite parts of the crystallization furnaces [3] some years later. An idea of the mechanism for generation of such so-called silicon carbide microdefects has been published in 1986 [12]. With the enormous growth of photovoltaic market beginning around the year 2000 also the need of cost effective mc-Si material for solar cells grew rapidly. The demand of Si feedstock for photovoltaic cells exceeded the production and Si for solar cells became a rare and expensive product around the year 2006 [13, 14]. This foiled the goal of cheap solar energy and forced the cell producers to use even low quality material, i.e. with a high amount of metallic and non-metallic impurities. This situation and the fact that mc-Si solar cells frequently showed so-called ohmic shunts, which have been significantly attributed to SiC precipitates [15–17], lead to enhanced research interest in this material and the carbon and nitrogen driven precipitates found there, to overcome the quality problems. To overcome Si shortage the capacity of conventional Si feedstock production using the Siemens process was increased and upgraded metallurgical grade (UMG) Si has been used for solar cell production [18–20]. In this material SiC and Si₃N₄ have been found as well and care was taken to avoid precipitates by using materials with low C and N content [18]. It was found that even high C and N content will not implicitly lead to SiC and Si₃N₄ precipitation, however special handling of the crystallization process is necessary then [21]. In the mid 2000s (just during the shortage period of Si feedstock) many findings about precipitates in mc-Si for solar cells have been made. Transmission infrared imaging and microscopy helped to identify particles within this material [22–24], which can be done at sawn wafers, but best image quality is obtained with polished wafers [25]. These findings helped to identify the contaminated parts in ingots and avoid their use for solar cell production. Not only SiC precipitates but also

Si_3N_4 precipitates have been found frequently [7, 15, 26]. The electrical properties of the precipitates and their effect on solar cell performance have been revealed by several authors [15, 17, 27, 28]. Analysis of the crystal structure of the precipitates and their contamination with trace elements have been carried out [29–32] helping to understand the growth mechanisms of precipitates. Details will be presented in Section 3.2. Nowadays nearly all carbon and nitrogen containing precipitates in p-type mc-Si are well investigated and most of their effects on solar cell performance as well as their effects on processes are understood. Though SiC and Si_3N_4 precipitates are still present even in state-of-the-art material [8], only a very small fraction of solar cells suffer from these precipitates since cell manufactures are aware of problems which may occur. Furthermore, Si feedstock is oversupplied these times, hence solar cells manufacturer are not forced to use low quality material and also requirements to impurity contents improved with respect to higher solar cell and module efficiencies. After IR inspection of the bricks before sawing, only the parts of the bricks being free of precipitates are sawed to wafers [24]. Nevertheless it is important to share the knowledge about these precipitates to hold the material quality as high as possible, which is even more important for the cell concepts emerging on the markets today such as mc-Si PERC (passivated emitter and rear) and n-type PERC cells.

3 Results

3.1 Growth and formation The formation of carbon and nitrogen correlated precipitates strongly depends on the thermodynamic conditions during the silicon crystallization and its process parameters. Local fluctuations in the melt such as temperature gradients, solidification velocity, influences of the process atmosphere, interaction with the crucible material, and the influence of impurities originating from the silicon feedstock or introduced through the process, affect the formation of non-metallic crystal phases – SiC and Si_3N_4 precipitates, see e.g. [3, 7,

26]. Namely two main types of SiC precipitates (filaments and particles), and three main types of Si_3N_4 precipitates (rods, fibers and nets) are distinguished, see Fig. 1 and Table 2 for more details. Since the solubility of elements in the melt is temperature dependent, its local distribution also affects precipitation. The solidification rate of the silicon, which is determined by the temperature gradient, specifies indirectly how heat and mass transfer can take place between solid and liquid phases of silicon [33]. The incorporation of carbon and nitrogen into silicon for multicrystalline crystallization do not originate primarily from the feedstock material. Additional contamination of the melt with nitrogen is mainly caused by the coating of the crucible with silicon nitride, which is partly dissolved by the liquid silicon during the crystallization process [6, 7, 29].

The carbon contamination may come from CO or CO_2 that is released into the crystallization atmosphere from the reaction of the graphite parts installed in the crystallization furnace with the silica crucibles [3]. Graphite boxes are used as retainer in furnaces to mechanically stabilize the silica crucible, which becomes soft at temperatures of about 1400 °C (i.e. the melting temperature of Si). Another possible source of CO is the reaction of residual oxygen or water vapor in the argon atmosphere with the graphite heaters. Moreover, it was described that oxygen in the Si melt evaporates at the top as SiO vapor, which is converted at the graphite cover of the crucible to CO [35, 36]. If CO or CO_2 comes in contact with the hot liquid Si, it dissolves and SiC and SiO are formed [3]. The carbon is captured by the Si melt, hence the carbon concentration of the liquid Si increases during the crystallization process [3, 7, 21, 37, 38]. The reactions between graphite parts, silica crucibles, and liquid Si have been investigated by [3] in detail.

The element specific distribution coefficient k_0 is determined by the solubility of an element in the liquid and solid phase of silicon. The Scheil equation [39] gives the concentration distribution of the crystallized ingot if the amount of the element dissolved in the liquid and solid

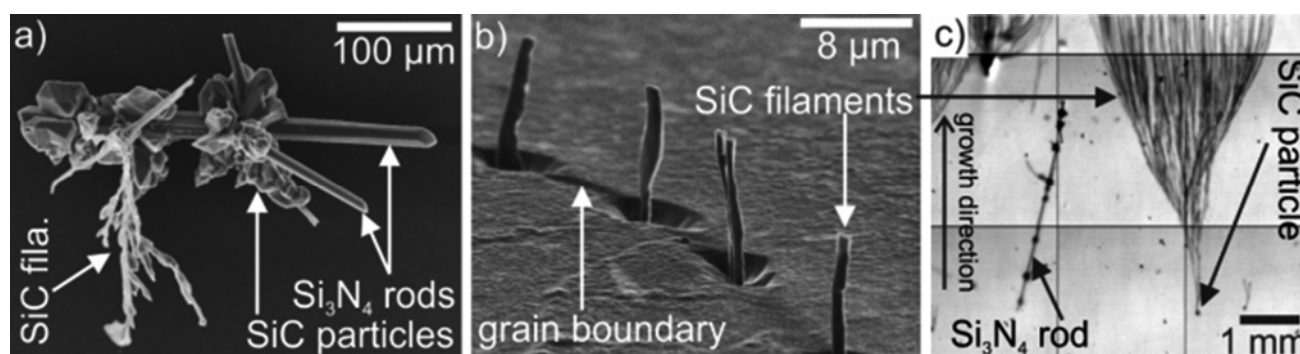


Figure 1 a) Scanning electron microscopy (SEM) image of secondary electrons (SE) of a conglomerate of Si_3N_4 rods, SiC particles, and SiC filaments. The precipitates in a) have been dissolved out of the bulk Si according to [7, 27], b) SEM SE image of single SiC filaments sticking out of the surface of a solar cell (etched-on surface according to [27, 34]) growing in a grain boundary. c) Transmission infrared (IR) microscopy image of a vertical slice (2 mm thick) cut out of a Si ingot with Si_3N_4 rods, SiC filaments and SiC particles. In c) the direction of growth of the ingot is given.

Table 1 Distribution coefficient and equilibrium solubility in liquid and solid silicon at crystallization temperature.

	k_0	$C_{L,Si} [10^{17} \text{ cm}^{-3}]$	$C_{S,Si} [10^{17} \text{ cm}^{-3}]$
C	0.07 ± 0.01 [40]	40 [41]	3.5 ± 0.4 [40]
N	0.00075 [42]	60 [42]	0.045 ± 0.01 [42]

does not change (no dissolution, evaporation and precipitation):

$$C_L = C_0 (1 + f_s)^{k-1}, \quad (1)$$

where f_s is the volume fraction of the already crystallized part of the ingot. C_L gives the concentration of an element in the liquid phase of Si. If C_S is the concentration in the solid phase, the ratio of C_S/C_L is called distribution coefficient k . At the condition $f_s = 0$ the parameter C_L is referred as C_0 and k becomes k_0 . The distribution coefficient as well as the saturation solubility for carbon and nitrogen in the liquid and solid silicon phase were investigated by many scientists and are summarized in Table 1.

The concentrations of C and N increase with progressive solidification front. If the solubility limit in the silicon melt is exceeded, precipitate formation occurs. If the solidification rate is sufficiently slow, it can be assumed that the phase boundary is almost in thermodynamic equilibrium. In addition, the gas management and thus the convection in the melt have an important influence. It determines how much the melt is mixed and how the output solidification heat is transported away. At too slow mixing of the liquid silicon compared to the solidification rate, a faster supersaturation of the melt can be expected and therefore an early formation of precipitates may occur as described in [38].

3.1.1 Formation of SiC particles and clusters

SiC particles show no preferred position in the grain structure of the ingot and can be found at different positions within the ingot, but mostly in regions close to the last crystallized part and close to crucible walls as a result of the heterogeneous nucleation process. SiC nuclei may form in the melt close to the phase boundary due to the segregation correlated increase of the concentration as a result of constitutional supercooling, implying local inhomogeneities in the carbon concentration in the liquid Si and temperature distribution. These nuclei may grow in the whole melt to SiC particles and clusters, i.e. conglomerates of SiC particles, in different sizes, if the carbon concentration exceeds the solubility limit. The SiC conglomerates are irregular arrangements of SiC crystals with statistical orientations. The individual vicinal faces of the single SiC crystal grains itself are very even and these are mostly highly perfect crystals [30], see also Fig. 1a. These observations and conclusions are consistent with [7, 26, 30, 34]. It is often observed that SiC particles grow at or around Si_3N_4 rods [26]. It is known that the Gibbs free energy of the formed precipitate in the Si melt is reduced in case of heterogene-

ous nucleation because less energy is needed for the SiC surface formation, hence Si_3N_4 rods are preferred places for SiC nucleation. This is also the case for the formation of SiC precipitates at the crucible wall. For the latter case also the presence of higher concentrations of impurities probably have an influence on the nucleation behavior. The cubic 3C-SiC or β -SiC crystal polytype can form at temperatures of about 1400 °C, it is also referred to as low-temperature type [43, 44]. All SiC precipitates found in solar silicon occur in this crystal polytype [30, 31]. Heine et al. [45] did some quantum mechanical calculations to explain why SiC preferably grows in this metastable cubic form and found out that the growth of this polytype is energetically more favorable, if donors are involved. As shown in [32, 46, 47] the most relevant donor within SiC is nitrogen (see Section 3.2.2 for more details).

3.1.2 Formation of SiC filaments Similar to SiC particles and clusters also SiC filaments grow in the cubic 3C-SiC type [15, 30]. The presence of nitrogen is most likely also in this case the limiting constraint as concluded in [45]. SiC filaments are mostly located at grain boundaries. The starting nucleation points of the filament growth are mostly SiC particles or clusters (see e.g. Fig. 1c). Two formation scenarios can be discussed. In the first one the grain boundary is already present and, with progress of the crystallization phase boundary, binding positions are increasingly offered to carbon or even small SiC particles. It is known that certain grain boundaries show a special rift shape at the solid-liquid phase interface [48]. If a SiC nucleation particle is trapped in this rift, the further growth of SiC filaments at the surfaces of the two meeting silicon grains can be easily explained due to the resulting reduced Gibbs free energy and the preferential carbon constitutional supercooling in this rift. The second considered scenario refers to the influence of an included SiC particle on the grain structure growth of the silicon itself. As known from float zone crystallization processes, the presence of incorporations within the silicon, like carbon, can lead to the formation of dislocations [49]. Therefore the presence of a SiC particle has to be considered as a massive disorder for the silicon crystal lattice, which may also lead to the formation of grain boundaries and establish the growth position of the SiC filaments and also gives the growth direction path. During the cooling of the grain structure in some cases a further accumulation of carbon due to diffusion processes may occur and consequently the non-uniform nitrogen distribution within the SiC filament cross section results, as reported in [47]. The habitus of the SiC filaments differs from that of the particles and clusters. They do not show any vicinal faces and they grow preferentially in crystallization direction, see Fig. 1c. Their crystallographic structure is microcrystalline and highly disturbed [30, 50], as can be seen in Fig. 3b. There was a controversy whether the filaments are growing in the liquid Si directly at the front of the crystallization plane (i.e. at the in-

interface between liquid and solid phase – interface model) or in the solid state shortly after crystallization [51, 52] by solid state diffusion of carbon. Growth of SiC filaments freely in the melt can be excluded since they are lying mostly in grain boundaries and branching upwards. If the filaments would grow completely in the melt and are then just overgrown, their crystallographic structure should not appear as disturbed as it is, but should be similar to that of the SiC particles, which was never observed so far. Note that the solubility of carbon in the Si solid is strongly temperature-dependent and reduces with reducing temperature [53]. Hence, even if carbon is introduced at the crystallization front at its solubility limit (see Table 1), with reducing temperature its concentration is above its solubility limit at this temperature and carbon tends to precipitate out. Then it strongly depends on the temperature history how much of the carbon may precipitate and how far it may diffuse. For temperatures below 1000 °C precipitation stops and the status freezes in. In [51] it has been estimated that carbon diffusion in the (solid) cooling Si crystal alone is not sufficient for transporting sufficient amounts of carbon to the filament sites. However, if in addition carbon diffusion in existing grain boundaries is considered, which should occur much faster than in the perfect Si crystal, this could explain an essential carbon transport to the already existing filaments in the solid. So far the growth mechanism of SiC filaments is assumed to be a mixture of growth at the interface of liquid to solid silicon and further thickness enhancement due to solid state diffusion of C towards the filaments in grain boundaries [50, 51]. The very first stages of filament growth may indeed occur in the melt directly at the solid-liquid interface, which is supported by the fact that the interface model [51] can explain the observed mean diameters and mean distances of the filaments. The continued thickness growth of the filaments by solid-phase diffusion is supported by the rough irregular SiC filament appearance and the observed high amount of crystal defects (see Fig. 3b) which do not need to be linked only to the contamination with nitrogen and other impurities.

3.1.3 Formation of Si_3N_4 rods The positions of Si_3N_4 rods show no preference within the grain structure of the crystallized silicon. In some cases Si_3N_4 rods can be found close to the crucible walls and the bottom, in the latter case it is assumed that there is a connection to the initial concentration of nitrogen within the silicon melt due to the crucible coating, and also the heterogeneous growth process probably have an impact at the walls. The rods can also be found in the last third of the crystallized silicon, which strongly depends on the crystallization conditions and the state of nitrogen segregation. Since Si_3N_4 rods are perfectly grown hexagonal rods, it is very likely that they grow in the liquid Si phase, where the growth is only weakly influenced by the surrounding. The supersaturation of nitrogen of the liquid Si is evident [7]. Si_3N_4 has a higher density (3.44 g/cm³) than liquid Si (2.55 g/cm³), hence Si_3N_4 rods

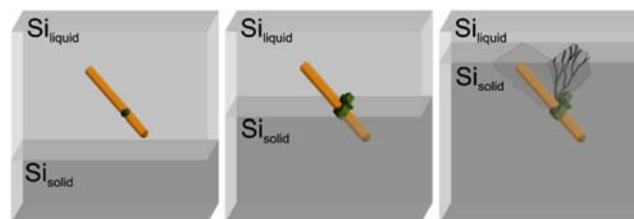
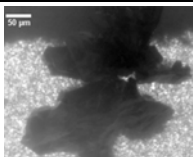

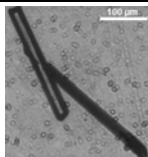
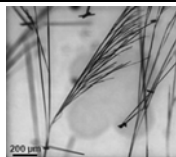
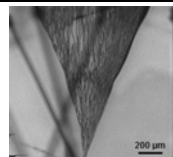


Figure 2 Model of the precipitate growth with an evolving Si_3N_4 rod formation in the melt (left) and successively growing SiC particles (center) and SiC filament growth in the presence of a grain boundary (right) (see Fig. 1a for comparison).

are sinking to the solid-liquid interface. However, convection currents in the liquid Si can force the growing Si_3N_4 to “swim” in the Si as long as they are still small and growing. In this stage of growth they also may become nuclei sites for the often observed attached SiC particles. With these observations it can be concluded that the Si_3N_4 rods are growing in the melt and their nuclei are formed due to constitutional supercooling probably close to the liquid-solid phase boundary. Figure 2 shows this procedure schematically in the area of solid-liquid phase boundary in the silicon crystallization. At the left image a Si_3N_4 rod has initially formed due to nitrogen supersaturation in front of the phase boundary. At the rod a SiC particle already starts growing. The Si_3N_4 rod and the SiC particle continue to grow in the melt (see Fig. 2 middle). After overgrowth (right) at the SiC particles the formation of grain boundaries occurs with progressive phase front. The growth of SiC filaments at these grain boundaries is starting from SiC particles as starting seed in the further silicon crystallization. The “capture” of the grain boundaries at the positions of the SiC particles is not considered here. It is assumed that the impact of the SiC particle and the resulting disturbance of the crystallographic lattice will influence the formation of grain boundaries, where the growth of SiC filaments will continue.

3.1.4 Formation of Si_3N_4 fibers Si_3N_4 fibers are generally oriented vertically and are branching in growth direction, and they show different crystallographic structure than rods (see Table 2). Hence they have another growth mechanism. However, the growth mechanism of Si_3N_4 fibers, see e.g. [34, 50] is not well known so far. Similar to Si_3N_4 rods also Si_3N_4 fibers can be detected within silicon grains and it is assumed that they are formed within the liquid silicon close to the solid-liquid interface. The presence of Si_3N_4 fibers can be often observed parallel to the presence of Si_3N_4 nets. This is the case for crystallization processes with a verified particular high nitrogen concentration. This precipitate type occurs in this case in a comparable high amount and preferential in the last crystallized third of the ingot, often at a particular height level. Due to the nitrogen segregation process, the concentration in the liquid phase is therefore particularly high and Si_3N_4 precipitates may also occur early depending on the crystallization rate [38]. Analogous to the SiC filaments, it is as

Table 2 Classification of carbon and nitrogen correlated precipitates in crystalline solar silicon.

type	SiC particles	SiC filaments	Si ₃ N ₄ rods	Si ₃ N ₄ fibers	Si ₃ N ₄ nets
IR microscopy					
size	1–600 μm in diameter	< 5 μm in diameter, up to 3 mm in length	< 30 μm in diameter, up to 2 mm in length	< 500 nm in diameter, up to 8 mm in length	< 500 nm in diameter, up to 3 mm in length
morphology	compact particles, frequently in clusters showing irregular surface and consisting of monocrystalline particles showing vicinal faces	irregular diameter, rough surface, multicrystalline	polygonal diameter, smooth surface, monocrystalline	steady diameter, smooth surface, monocrystalline	irregular diameter, smooth surface, multicrystalline
local growth preference	within grain volume, often at Si ₃ N ₄ rods	mostly in grain boundaries, growing in crystallization direction	within grain volume, random orientation	within grain volume, growing in crystallization direction, branching	in grain boundaries, growing in crystallization direction
crystal structure	cubic, β-SiC	cubic, β-SiC	hexagonal, β-Si ₃ N ₄	trigonal, α-Si ₃ N ₄	trigonal, α-Si ₃ N ₄
space group	F43m (216)	F43m (216)	P63 (173)	P31c (159)	P31c (159)
lattice constants	$a = 0.436$ nm	$a = 0.436$ nm	$a = 0.760$ nm, $c = 0.291$ nm	$a = 0.775$ nm, $c = 0.562$ nm	$a = 0.775$ nm, $c = 0.562$ nm
impurities	N, Al	N, O	Li, C, O, Mg, Ca	C, O, Ca	C, O, Al, Ca
electrical resistance	$8.17 \times 10^{-5} \Omega$ cm (4PP)	$2 \times 10^{-3} \Omega$ cm (4PP) [28]	$> 4.7 \times 10^7 \Omega$ cm (4PP) [28]	$(5 \pm 4) \times 10^8 \Omega$ cm (2PP)	$(1.44 \pm 0.26) \times 10^{10} \Omega$ cm (2PP)

sumed that Si₃N₄ fibers also need an initial seed for their growth. According to observations via IR microscopy the initial seed consist of smaller Si₃N₄ precipitates [50]. Like Si₃N₄ rods, these are enclosed by the solidifying silicon melt within the silicon grain structure. Si₃N₄ fibers often occur in bundles, which have a preferred orientation with an angle below 45° perpendicular to the direction of crystallization front, which is an indication that they grow immediately in front of the liquid-solid phase front and do not swim unaligned in the melt. The cross-section of the fibers is often observed as V-shaped or in the form of two narrow angled surfaces. In many cases connected fiber segments show an angle of ~120°, which is also the outer angle observed for the hexagonal Si₃N₄ rods. Therefore a correlation of certain crystal axes within the silicon could be suspected, along which the single-crystal fibers grow preferentially within a silicon grain with the crystallization front, since in this case the mismatch of the crystal lattice is lowest. In [26] an alternative growth process was proposed. It was assumed that a liquid iron silicide particle (droplet), which is formed at the solid-liquid interface, is the nucleus for the Si₃N₄ fibers. However, there is no experimental evidence of any FeSi₂ particles at the starting points of Si₃N₄ fibers. So this growth model is very unlikely from our knowledge so far.

3.1.5 Formation of Si₃N₄ nets Similar to SiC filaments, also Si₃N₄ nets can be observed at silicon grain boundaries and the growth is assumed close to the liquid-solid phase boundary with processing crystallization front. Due to the lower hardness differences between Si and Si₃N₄ it is supposed that the starting seeds of the net growth are mostly enclosed by already growing silicon grain boundaries. There are also observations showing the simultaneous growth of SiC filaments and Si₃N₄ nets in the same grain boundary [54]. As for the Si₃N₄ fibers, the starting seeds are smaller Si₃N₄ precipitates [50]. The morphology shows that this starting seeds are Si₃N₄ fibers. As clearly visible especially for the Si₃N₄ nets, the growth takes place in a certain crystallization height. In Section 3.1.4 it was mentioned that the growth takes often place in parallel to the presence of Si₃N₄ fibers in a high nitrogen concentration silicon environment and a high degree of constitutional supercooling close to the phase boundary. Consequently, at a certain time in the crystallization process simultaneously a high concentration of nitrogen and a high degree of constitutional supercooling has to be present for the formation process.

3.2 Structural, chemical and electrical properties A classification of all known carbon and nitrogen cor-

related precipitates in crystalline solar silicon is presented here by criteria of structure (morphologic/microscopic as well as crystal structure properties), chemical composition, and electrical properties. These precipitate specific material properties are described in detail in the following Sections 3.2.1–3.2.3. A deduced classification is presented in Table 2.

3.2.1 Structural properties The known precipitation types can be distinguished already by their morphologic appearance using the IR microscopy in transmission mode as presented in [7, 26, 32, 55–57]. In the following, the morphologic structure visible in transmission IR microscopy of each precipitate type is presented, followed by the results of their corresponding crystallographic polytype which are linked to representative TEM/SAED measurements (see Fig. 3).

SiC precipitates are often found as compact particles, which are frequently clustered. The SiC clusters show an irregular surface, but on a closer look (e.g. via SEM/TEM) it is visible that they consist of monocrystalline particles showing vicinal faces [7, 55]. Often individual particles have grown together to form a compact (multi) crystalline SiC cluster particle [7, 55]. The diameter of SiC particles and clusters can range up to 600 μm . The crystallographic polytype of SiC particles show the cubic 3C-SiC phase (also called β -SiC) with a lattice constant of $a = 0.436 \text{ nm}$ (see also Fig. 3a and Table 2) [7, 30]. SiC filaments appear with irregular diameters around 1–5 μm in size with a length up to several mm [26, 30, 55]. SiC filaments show a rough surface which also matches the irregular growth behavior within grain boundaries. Cross sections prepared for TEM investigations show a poly crystalline character and this is also assumed for the length growth [30]. Like the SiC particles also SiC filaments grow in the 3C-SiC phase (see Fig. 3b). In contrast to the SiC particles much more crystal defects as stacking faults or dislocations can be observed within the filaments [30, 50]. This is due to their different growth mechanism (see Section 3.1.2) and is also linked and discussed with respect to the impurity level (see Section 3.2.2).

Si_3N_4 rods are monocrystalline showing a polygonal mostly hexagonal cross section with pyramidal formed capping regions with smooth surfaces [7, 55]. In optical microscopy the rods often appear yellowish transparent with $<30 \mu\text{m}$ in diameter and up to 2 mm in length [26, 55, 58]. They grow in the hexagonal β - Si_3N_4 polytype with the lattice constants $a = 0.760 \text{ nm}$ and $c = 0.291 \text{ nm}$ (see Fig. 3c) [7, 55]. Normally Si_3N_4 rods are massive, however frequently Si_3N_4 rods are found, which are hollow and filled with Si, see e.g. [58].

Si_3N_4 fibers only grow with small diameters $<500 \text{ nm}$ but can reach length up to 8 mm [34, 55]. They show steady diameters with a smooth surface and a monocrystalline character. In IR microscopy they are often visible as bundles with a connection to the seed starting point. Si_3N_4 fibers as well as Si_3N_4 nets are formed in the trigonal α - Si_3N_4 polytype (see Fig. 3d, e) with $a = 0.775 \text{ nm}$ and $c = 0.562 \text{ nm}$.

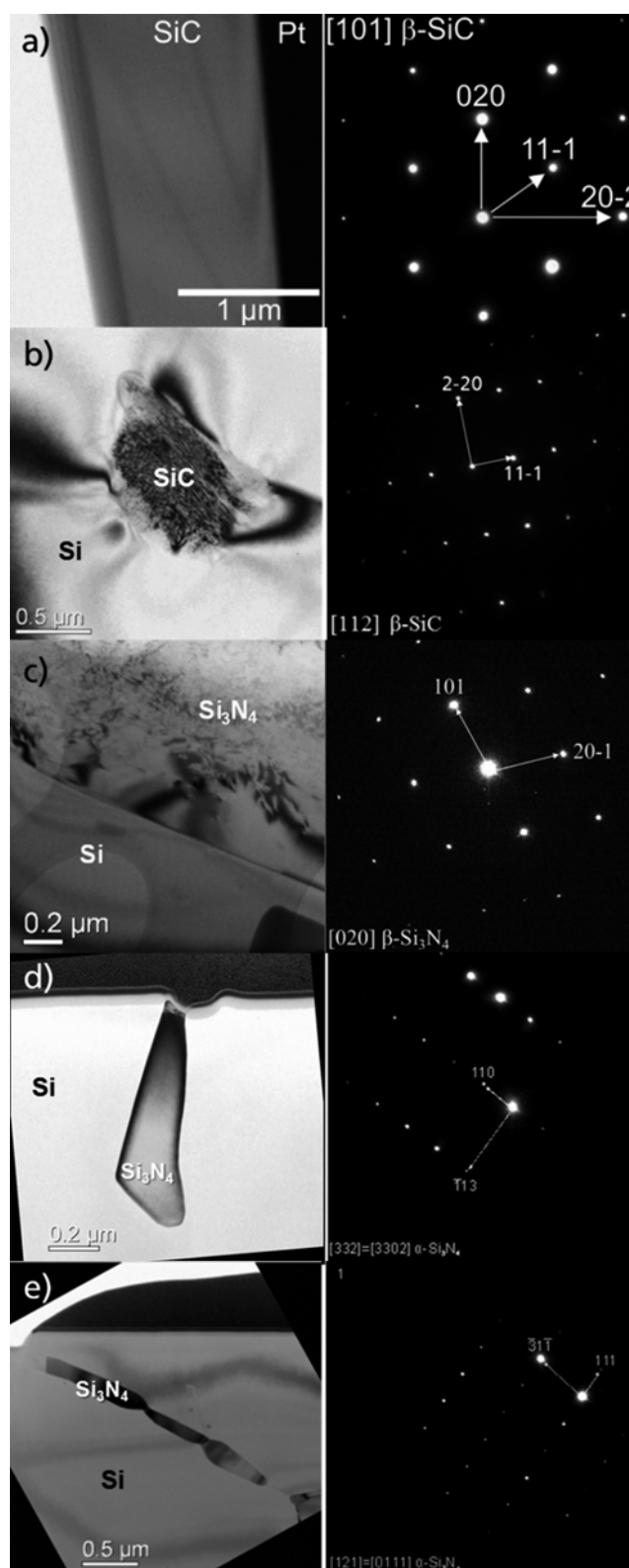


Figure 3 Bright field TEM lamella sections with corresponding SAED patterns for an a) SiC particle [30], b) SiC filament [31], c) Si_3N_4 rod [31], d) Si_3N_4 fiber [57] and e) Si_3N_4 net [57].

In contrast to the fibers, the nets show an irregular diameter, also with a smooth surface, but a multicrystalline length growth. Si_3N_4 nets are often very branched and also have small diameters of <500 nm with up to 3 mm in length. The correlation of Si_3N_4 to the possible formation type and the involvement of impurities are described in Section 3.2.2.

3.2.2 Chemical properties In the following the known chemical properties from literature and our latest results concerning composition and trace elements within the different precipitates are summarized, as well as the getter effect of some precipitates.

Due to the determined crystal polytypes of the precipitates also the stoichiometry is very well defined for the always cubic SiC precipitates and also for Si_3N_4 precipitates in the trigonal or hexagonal polytype. What needs to be cleared up are therefore the individual impurity level and the possibility of easy chemical distinctness. This can be reached via the method of time-of-flight secondary ion mass spectrometry (ToF-SIMS) as presented in [31, 32, 50] and the observation of only a few signals for all precipitates containing main components of C, N and O. By chosen characteristic ion cluster intensities in negative ion mode and usage of Cs^+ sputter source, signals for C, O, CN, SiC, SiN are sufficient to distinguish the different precipitates. Figure 4 shows the results of the ion intensities after normalization to the total ion yield of individual ROIs of the ToF-SIMS measurements for each precipitate type.

Using a relative sensitivity factor (RSF) determined by an ion implanted standard sample, the N concentration within several individual investigated SiC particles was determined to be in the range between 4.3×10^{20} and 2.3×10^{21} atoms/cm³. For SiC filaments the N concentration was found to be even higher and is determined to be in the range between 1.3×10^{21} and 2.8×10^{21} atoms/cm³. Due to the small diameters and the limited lateral resolution of ToF-SIMS – even in the used HR-ToF-SIMS mode [50] – the influence of the surrounding Si signal is as

summed to cause an underrating of the real N content within the SiC filament. As can be seen in Fig. 4, Si_3N_4 precipitates contain carbon as well as oxygen. There is a certain fluctuation of the intensities of C and O and especially for Si_3N_4 rods, the O content varies, but compared to the other Si_3N_4 types, the oxygen shows the highest intensities within the rods.

Using Eq. (2) with the ToF-SIMS ion intensities for I_{SiC} and I_{SiN} , a quick phenomenological distinction in SiC like or SiN like precipitate type can be reached:

$$\Delta I = \frac{I_{\text{SiC}} - I_{\text{SiN}}}{I_{\text{SiC}} + I_{\text{SiN}}} \quad (2)$$

If the value for ΔI is ≤ 0.8 , a Si_3N_4 type is present, for values > 0 SiC is present (SiC filaments are often close to $\Delta I = 0$).

It was shown in [31, 32, 46] that SiC filaments and particles contain a high amount of nitrogen, and in [47] a further quantitative chemical analysis on microscopic scale revealed that the SiC filaments are a $\text{Si}_1\text{C}_{1-x}\text{N}_x$, with x up to 0.3, which in turn is a concentration of about 15 at% nitrogen. Hence, it was assumed in [47] that the N-doping must be even higher than given in [28]. However, it has to be emphasized that there is no silicon carbon nitride polytype present, which would have other crystallographic properties and only the cubic SiC polytype was detected in all experiments (see Section 3.2.1). In all cases a solid solution of N in SiC is observed. However, due to different growth parameters of mc-Si blocks their nitrogen content may vary strongly, hence the variation of the nitrogen concentration in SiC filaments may be very great as well, e.g. due to different growth rates, see e.g. [38].

Next to general distinction also trace elements are investigated via ToF-SIMS (see Fig. 5). These analyses are performed in positive ion mode using the O_2^+ sputter source. The results are shown in Fig. 5 as lateral resolved ion images for the individual detectable elements next to a microscopic image of the analyzed precipitates. Si_3N_4 rods show signals for Li and Mg. On the interface between SiC particle and Si matrix, Al was found as reported in [59]. In many cases for the rods also signals for Na, Ca and K are detected [26, 32]. For SiC filaments no further elements than N and O are detected. Si_3N_4 fibers contain Ca as trace element. Within Si_3N_4 nets the elements Al and Ca are detectable with ToF-SIMS. The presence of alkali metals is an often reproducible result and is therefore considered as characteristic chemical property. SiC-like precipitates appear to have a preference for attachment of metals. With ToF-SIMS, this could only be detected for Al. Other works also brought evidence of Cu, Ni and Fe for SiC particles by synchrotron based X-ray fluorescence microscopy (μ -XRF), X-ray absorption micro-spectroscopy (μ -XAS), and energy dispersive X-ray spectroscopy (EDX) [60–62]. Not all, but frequently found impurities are also shown in Table 2, but note that the diversity of detectable impurities within the precipitates is also process depending.

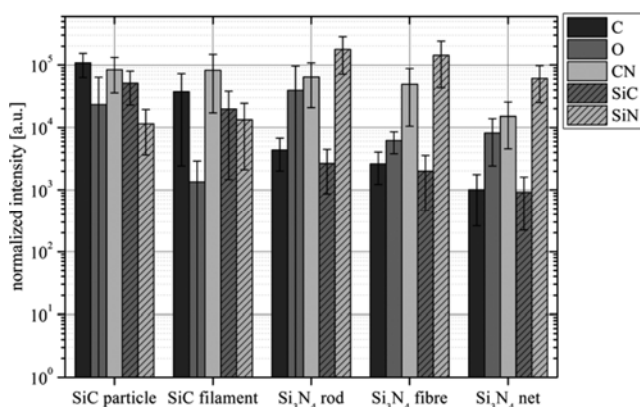


Figure 4 Chemical classification of precipitate types after statistical evaluation of characteristic ToF-SIMS mass peaks (negative ion mode).

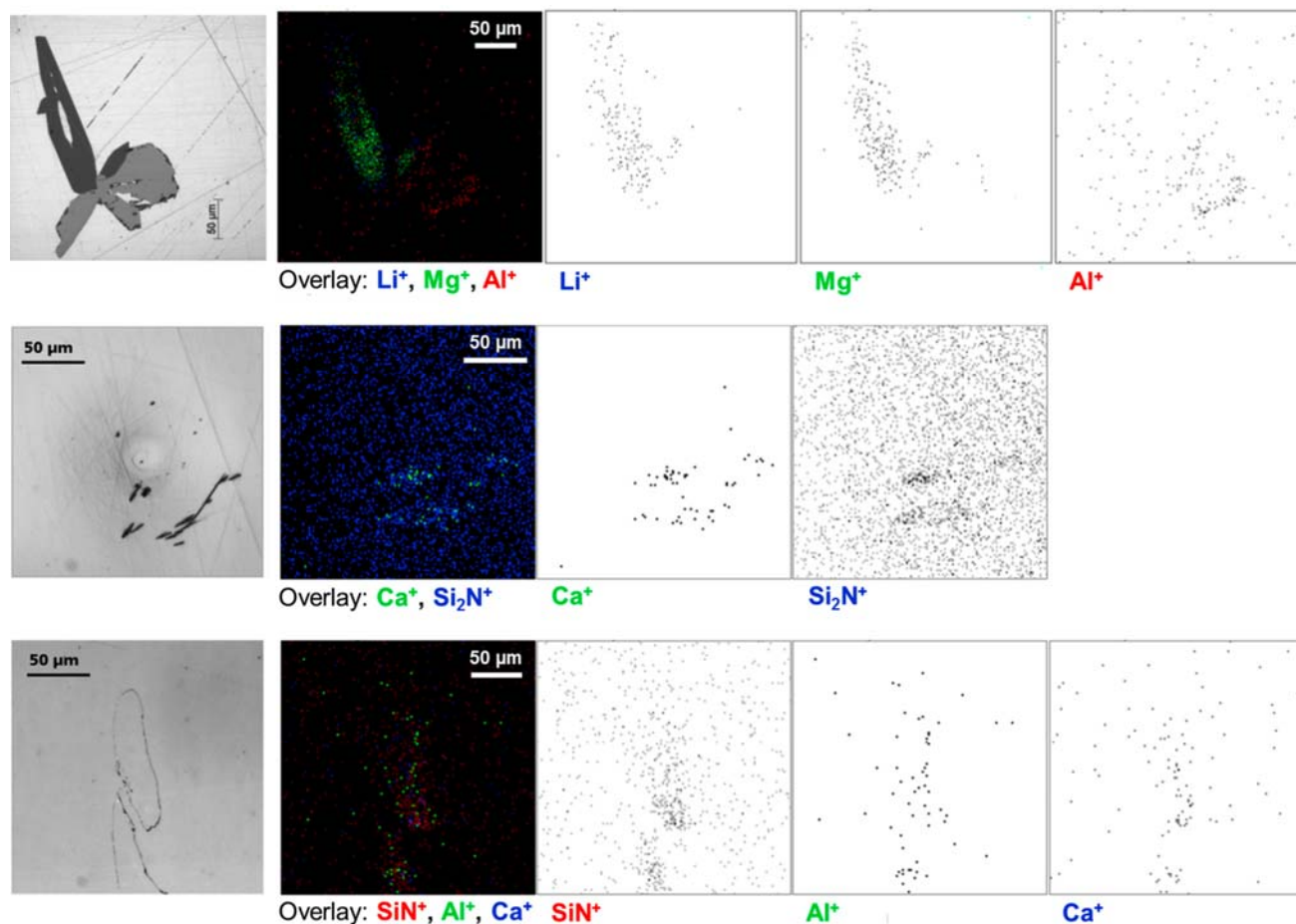


Figure 5 Light microscopic position (first column) of positive ToF-SIMS ion images of detectable trace elements of SiC particles with Si_3N_4 rod (top row), of Si_3N_4 fibers (center row) and of a Si_3N_4 net (bottom row). The second column shows the overlay of the detected ion species, which are shown separately on the right in each row. Scale bars in the second column hold for the whole row, respectively.

In addition to ToF-SIMS analysis, trace elements were also investigated by inductively coupled plasma mass spectrometry (ICP-MS) of a vertical cut slice with predominantly containing Si_3N_4 precipitates in the capping region (last crystallized part of a VGF mc-Si ingot). The silicon slice was cut in six vertical samples (see Fig. 6, left) of the size of $0.4 \times 3.0 \times 0.19 \text{ cm}^3$ and decomposed by the chemical vapor phase decomposition (VPD) method [63] using a solution of HNO_3 (65%), HF (48%) and H_2SO_4 (96%). The precipitates remained undissolved in the analytic solution, which was diluted and analyzed by ICP-MS. Figure 6 shows the sample regions and the quantified concentrations for the depicted elements and the corresponding limit of detection (LOD).

Regarding the segregation process during crystallization, the expectation is to find higher concentrations within subsequent crystallization parts, as observed for samples 1 to 4. In contrast, samples 5 and 6 which contained the undissolved precipitates show reduced concentrations for the elements Na, Mg, K, Ca, Ti, Mn, Ni and Zn. Hence it can be concluded that these elements are still in the undis-

solved precipitates and were reduced in the silicon matrix, therefore the getter effect can indirectly be proven for in this case predominately present Si_3N_4 precipitates. Some of these elements as Ca, Mg or K were also found to be pre-

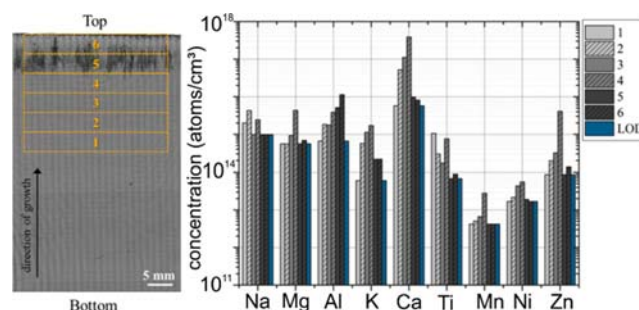


Figure 6 IR imaging of top region of a silicon ingot containing Si_3N_4 fibers and nets with marked samples 1–6 (left, the arrow points to the direction of growth); quantitative impurity concentrations analyzed via ICP-MS shows getter effect for several elements due to insolubility of precipitates in VPD method (right). The blue LOD bar gives the limit of detection for each element.

sent in different Si_3N_4 precipitates via ToF-SIMS. The Al concentration, which was detected at some precipitate positions with ToF-SIMS, is not reduced for samples 5 and 6, which could be explained by the fact that Al rather attaches to the precipitates and the surrounding crystal defects and is not incorporated primarily in the precipitates.

3.2.3 Electrical properties of SiC and Si_3N_4 precipitates Linear shunts in solar cells are detrimental to the performance of the cells. The reason for ohmic (i.e. linear I - V characteristic) shunts is a short circuit between the front side, i.e. the highly doped emitter or front metal grid, and the backside or bulk, i.e. the back surface field (BSF) or the back contact [16]. Linear shunts can be easily determined by dark lock-in thermography (DLIT), because they show the same lock-in signal amplitude under forward and reverse bias [16, 64, 65]. This is shown in Fig. 7: in a)

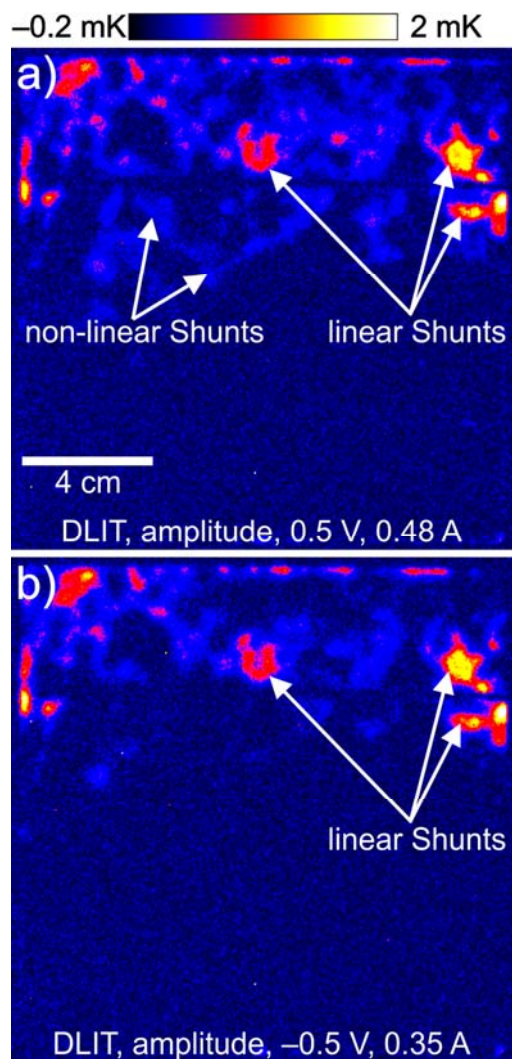


Figure 7 DLIT images showing the typical signal pattern of linear shunts due to SiC filaments. a) DLIT amplitude image of a solar cell at 0.5 V forward bias, b) DLIT amplitude image of the same cell at -0.5 V reverse bias.

the amplitude DLIT image of an Al-BSF screen printed mc-Si solar cell at 0.5 V forward bias exemplarily shown. In b) the corresponding -0.5 V reverse bias amplitude DLIT picture is displayed. All linear shunts show nearly the same signal strength in forward and reverse bias. Some non-linear shunts are only visible at forward bias. There are some trivial causes leading to linear shunts, which are all process related. These are for instance badly opened edges of the solar cells, cracks which are filled with Al paste or Al particles on the front side [16].

In 2002 Rakotoniana et al. reported about material induced linear shunts in multicrystalline silicon solar cells [15]. It was shown there that SiC precipitates are the cause of the short circuit leading to shunting. Indeed the linear shunts shown in Fig. 7 are caused by massive SiC filament precipitation in the Si block used for this solar cell. These filaments may cause severe linear shunting, because they can reach some mm in length and therefore can penetrate one wafer in the whole or even more wafers and may short front and rear contact of the solar cells [16, 17, 26]. This is shown schematically in Fig. 8a and b. Using electron-beam induced-current (EBIC) imaging, SiC shunts can be experimentally verified at bare solar cells by their dark contrast at grain boundaries (GB) as is shown in Fig. 8c, where exemplarily an EBIC image taken in the geometry of a) is shown. Taking EBIC images from the rear side (the

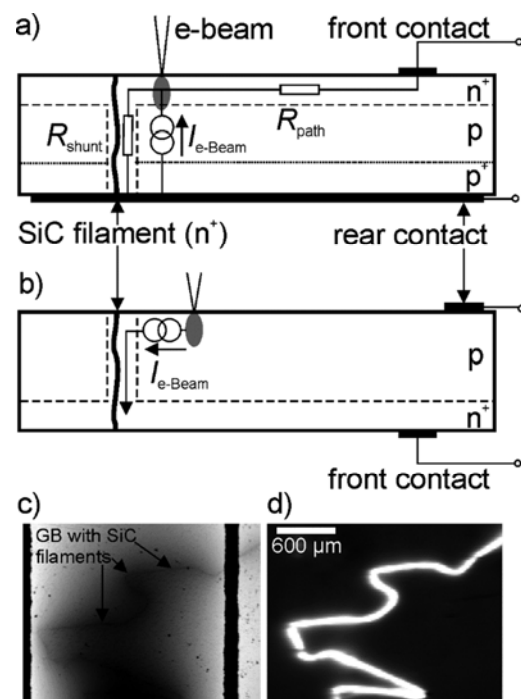


Figure 8 Model of the shunt formation of SiC filaments in Si solar cells and EBIC signal formation for different sample preparations, a) EBIC at the solar cell's front side [a sample image is shown in c)]. b) EBIC at the rear (BS-EBIC) of the cell as shown in d) and e.g. [17, 69]. Most of the rear aluminum contact was etched or polished away, only a small part was left over for EBIC probing (images in a) and b) adopted from [69]).

rear contact is removed), as sketched in Fig. 8b, the EBIC contrast inverts, as is shown for this sample in Fig. 8d. Note that in these low-resolution images the closely lying SiC filaments in the grain boundary appear as a continuous line.

When SiC filaments were identified for the first time, they were assumed to be particles and their conduction mechanism in grain boundaries was not clear. Initially the shunting mechanism was explained by assuming an inversion of the p-type material at the interface between the SiC precipitates and the Si bulk in [15, 16].

This conduction mechanism was proposed at the same time by Hahn et al. to explain high J_{sc} currents in RGS (ribbon growth on substrate) solar cells [66], which have been measured in this material in spite of low lifetimes. However, in the case of RGS solar cells the inversion channels have been found to be formed by oxygen precipitates at dislocations leading to local inversion of the p-type doped Si at the interface between the oxygen precipitates and the bulk Si and therewith to a high conductivity of this interface [66, 67]. In [15] it was assumed that the inversion in SiC containing grain boundaries would be due to the large carbon concentration close to that interface.

It is interesting to note that SiC filaments have been found already in 2000 in RGS material, but no shunting of the solar cells was reported at that time and in this specific material [68]. In 2007 it was revealed by direct measurements of the resistivity at SiC filaments separated from the bulk that the SiC filaments themselves are highly conductive and n-type with a doping density in the order of 10^{18} cm^{-3} [28]. It was estimated there that the conductivity of an inversion layer would be not high enough to explain the shunting activity. The resistivity of SiC filaments was determined to be in the low $10^{-3} \Omega \text{ cm}$ range, which fits, regarding the many parallel conducting SiC filaments, to the shunt resistance measured on cell level of only some Ω [28]. The doping was assumed to be due to the nitrogen, which is a shallow donor in SiC, and whose concentration is relatively high within the SiC (see Section 3.2.2) [28] and reaches concentrations in mc-Si of $< 3 \times 10^{16} \text{ atoms/cm}^3$ [50]. In Fig. 9a a 2-point-probe measurement of a single SiC filament, which was separated from the bulk of a solar cell, is shown (reproduction from [28]). The current–voltage (I – V) curve measured at this SiC filament shown below is linear and the resistance was determined to about 15Ω in this case.

In principle also SiC particles may cause shunting, since they are highly n-conducting as well. Since the diameter is often below the wafer thickness (see Table 2), shunting due to SiC clusters or crystallites is more unlikely but not impossible, in particular for thin solar cells and/or if neighboring clusters touch each other yielding a cluster chain. In general ohmic shunting is only expected if n-conducting precipitates touch both, the front and the rear contact [50, 55]. Hence, no ohmic shunting is expected for SiC filaments which do not reach both solar cell contacts and if filaments are very thin or even interrupted [70]. It

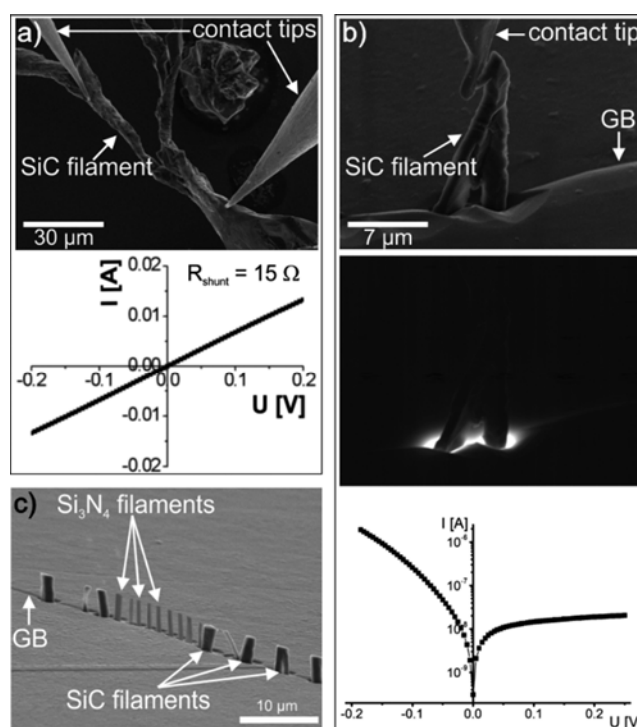


Figure 9 a) Top: SEM SE image of a 2-point-probe measurement of a single SiC filament; bottom: I – V curve of the 2-point-probe measurement showing a linear behavior with a resistance of about 15Ω . b) Top: SEM SE image of a 2-point-probe measurement of a n^+ -doped SiC filament embedded in the p-doped Si bulk; middle: BS-EBIC image of the SiC filament; bottom: I – V curve of the hetero n^+p junction (SiC filament – Si bulk). c) SEM SE micrograph of a grain boundary in mc-Si solar cell containing conducting SiC and non-conducting Si_3N_4 filaments (equivalent to Si_3N_4 nets).

was speculated as well that an insufficient contact of the SiC filaments to the front or back side of the solar cell may hinder shunting [71], however this could not be proven in any reference so far.

The bandgap of pure SiC is about 2.4 eV [56] and that of Si about 1.1 eV at room temperature. Hence, the contact between n^+ -doped SiC filament and p-doped Si bulk is a typical hetero p–n-junction between two semiconductors. Its voltage–current curve is indeed non-linear as shown in Fig. 9b (bottom, reproduction from [28]), here the I – V curve was measured between the p-Si bulk and a single SiC filament probed by a PtIr tip [34], see Fig. 9b, top. Hence, electronically there is a collecting barrier at this p–n-junction, which can be imaged by electron-beam induced-current (EBIC) as it is shown in Fig. 9b in the middle, and in e.g. [69, 71]. By fitting measured I – V and C – V characteristics of an electrically isolated SiC filament in p-Si bulk material to an AFORS-HET model [72], the band-offset of this heterojunction was determined in [28] to be positive with a barrier height of about 50 meV by simulations. Hence electrons can easily overcome this barrier and an inversion layer is extremely unlikely, in turn the shunt cur-

rent flows in the SiC filaments [28]. In [73] it was calculated that the bandgap of SiC might be reduced down to 1.2 eV and the SiC turns from an indirect semiconductor to a direct one due to high doping. The SiC filaments behave then like a metal concerning the conductivity; hence the heterojunction barrier between SiC and Si might be even lower or reaching flat band conditions, with the consequence that the shunt current path inside the SiC filaments becomes even more likely (see Section 4).

The electronic activity of Si_3N_4 precipitates is described in [16, 28, 31, 34, 50]. It was found that nearly all Si_3N_4 structures are insulating [28, 34] or show a somewhat unclear electrical behavior [16, 31]. In [34] it was shown that conductive SiC filaments and non-conductive Si_3N_4 nets may exist in one and the same grain boundary side by side. In Fig. 9c a scanning electron microscope (SEM) micrograph of such a grain boundary containing SiC filaments and Si_3N_4 net filaments is shown. The electrically isolating Si_3N_4 net filaments are significantly thinner than the highly conducting SiC filaments and show a much smoother surface [34]. The resistivity of Si_3N_4 rods was given to be in the order of $10^7 \Omega \text{ cm}$ in [28], hence they are not electrically active, and are in most cases not detrimental to the solar cells performance since they do not cause linear shunts. However, in [16] it was reported that non-linear shunts are formed at macroscopic Si_3N_4 precipitates. Please note that these kinds of shunts are not linear shunts as they are caused by SiC filaments described above, instead it was assumed that the non-linear shunts are caused by high recombination at the interface between the precipitate and the Si bulk [16]. In [31] it was also reported that a Si_3N_4 rod may cause a shunt, a linear shunting mechanism was not strictly excluded due to the fact that an EBIC signal could be measured at the interface between the Si_3N_4 rod and Si bulk as shown in Fig. 10. Due to the high determined oxygen content for this individual Si_3N_4 rod also a n-type doping was present. This EBIC characteristic was analogous qualitatively observed also for the heterojunctions of SiC precipitates to the p-Si bulk (see e.g. [28]). However, it is not clear from [31] whether the observed shunts are linear ones since the also shown single DLIT image is insufficient to prove the linear shunt behavior. It has to be mentioned that the investigated Si_3N_4 rod is accompanied by SiC clusters, which might be also responsible for shunting if their dimensions are big enough.

In the course of this work presented here, it turned out that the position of the Si_3N_4 rod and the shunt presented in [31] do not exactly coincide. However, the EBIC signal at the rod shown in [31] and Fig. 10 is evident; hence a certain although very weak electrical activity is present. The resistivity of Si_3N_4 precipitates is always hard to measure due to high contact resistances and challenge of current injection. So it is also likely that the front and rear contact of the solar cell are sufficient to contact these precipitates for shunting losses. In Table 2 it is shown that the conductance of Si_3N_4 rods is very low, however there are differences in the order of up to a factor of 1000. These differences can

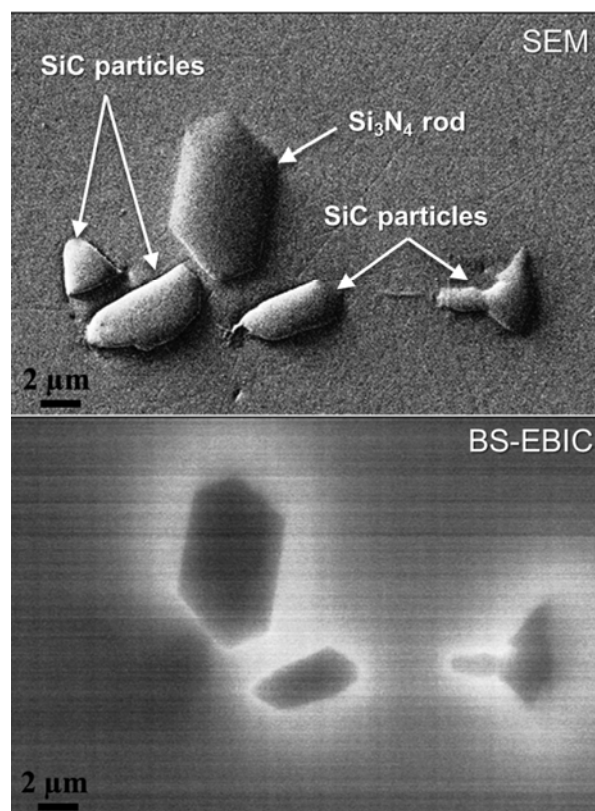


Figure 10 SEM (upper) and BS-EBIC (lower) image of a Si_3N_4 rod accompanied by SiC particles.

be explained by doping, which may vary strongly [50]. The increased EBIC signal could also be explained as follows: if during the EBIC measurement the electron beam comes close to the Si_3N_4 rod, electrons are captured by the rod, the rod is charged negatively and an inversion layer is formed at the interface between the rod and the p-doped Si bulk. Electrons can now easily travel along this inversion layer to the emitter leading to an increased EBIC current, which results in the positive signal at the rod as shown in Fig. 10 and in [31]. Note that typical EBIC currents are in the μA range and orders of magnitude smaller than the currents in the mA range, which are connected with linear (ohmic) shunts.

Wrapping up the electronic properties of SiC and Si_3N_4 precipitates in mc-Si it is obvious that SiC precipitates are very harmful to solar cells performance. Especially highly conductive SiC filaments may cause severe shunts, and, since they can be up to several mm long in the direction of crystallization, they may harm several adjacent wafers. Si_3N_4 precipitates are insulating and therefore usually not harmful to solar cells. This was shown for Si_3N_4 rods and Si_3N_4 nets [28, 34]. However, some rare reports about non-linear shunts caused by macroscopic Si_3N_4 precipitates can be found in Refs. [16, 31]. Si_3N_4 rods may show a slight electronic activity [31], but their influence on the I - V characteristic of the solar cell is negligible. Therefore Si_3N_4 rods can be classified as harmless to solar cells regarding

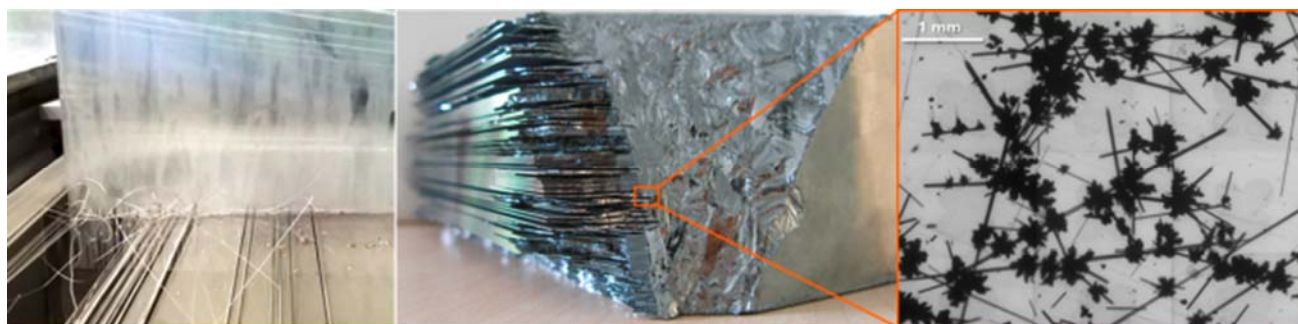


Figure 11 Wire rupture during sawing process (left) due to massive amount of SiC particles and Si₃N₄ rods within the silicon ingot visible by IR transmission microscopy of cracked out mc-Si wafer fragments (see middle and right).

the electrical properties. However, extended precipitates, even if insulating, which reach both solar cell contacts and might be decorated by impurities (see Section 3.2.2) and surrounded by decorated dislocations may cause electrical losses in terms of recombination and breakdown effects as known from decorated grain boundaries [3–5].

3.2.4 Mechanical properties of SiC and Si₃N₄ precipitates SiC is a very hard material with hardness after Vickers and Knoop of 21 GPa to 25 GPa [74]. The hardness of pure crystalline β -Si₃N₄ was given to be about 20 GPa (at 500 g load) and that of pure crystalline α -Si₃N₄ was given to be about 34 GPa (at 200 g load) [75]. However, in the case of β -Si₃N₄ a small amount of iron (approx. 0.1 wt%) reduce the hardness drastically to about 13 GPa [75], which is important to note since in most mc-Si materials iron is existent and was also observed directly in β -Si₃N₄ rods [26, 29, 32].

Si has a hardness of 11 GPa to 14 GPa [76, 77]. Si bricks are typically cut into wafers with a wire saw using metal wire and slurry containing small SiC particles (approx. 10 μ m diameter) as abrasive [78]. Since SiC and Si₃N₄ precipitates are harder than Si, these precipitates in the block may lead to wire rupture (see Fig. 11, left), saw marks, cracks, and scratches on the surface of the wafers [79, 80].

Especially SiC crystallites in mc-Si may reach diameters up to several 10 μ m or may even cluster to structures up to 0.5 mm in diameter [7, 30, 32, 79, 80]. Therefore the sawing process may be hindered by SiC particles leading to increased wire tension and unwanted wire movement since the wire is deflected by the SiC particle leading to above mentioned problems on the wafer or even wire rupture [79, 80] (see Fig. 11, right). Si₃N₄ rods, which are present in the β -phase of Si₃N₄, and therewith are softer than the SiC slurry particles, are cut with no problems [79, 80].

Only if very massive agglomerations of Si₃N₄ rods are existent in the mc-Si block, they may lead to problems during wafering. Silicon nitride fibers and nets consist of α -Si₃N₄. Since the α -phase of Si₃N₄ is harder than the β -phase [75, 81] one would expect difficulties with these precipitates during wafering as well. However, α -Si₃N₄ fibers and nets are very thin exceeding not more than

100 nm to 500 nm in thickness (see Table 2) and are therefore easy to cut; indeed no problems caused by α -Si₃N₄ or β -Si₃N₄ precipitates have been observed during wafering [79, 80].

There are some findings in literature suggesting that SiC precipitates weaken the mechanical strength of silicon solar cells. Stress measurements on material containing SiC and Si₃N₄ precipitates have been performed by optical methods like infrared birefringence imaging (IBI) [61, 82]. Finite element calculations to the same topic have been published at the same time [61, 82, 83]. The average tensile stress (σ_1 – σ_2) was reported to be about 24 MPa at the β -SiC/Si interface and 12 MPa at the β -Si₃N₄/Si interface [61]. It was stated that the radial tensile stresses around β -SiC particles are due to the mismatch of the coefficients of thermal expansion between SiC/Si₃N₄ and Si [61, 82, 83]. It was concluded in [61] that these stresses are strong enough to result in a lower mechanical yield of affected Si wafers mainly due to β -SiC particles. Furthermore, it was concluded in [61] that such stresses can explain the getter effect in the vicinity of SiC precipitates as well the fact that SiC particles may serve as nucleation points for dislocations and extended defects.

4 Discussion Regarding the material properties of the precipitates most investigations and resulting estimations of their effects are made for boron doped p-type silicon and the conventional p-type Si solar cell concept with phosphorous doped n^+ emitter. Nowadays, there are several new cell concepts (e.g. PERC) and also concepts based on n-type silicon material and with a more complicated electrical setup. Since the crystallization process is not changed by the choice of the doping element regarding the formation process of SiC and Si₃N₄ precipitates and their material properties, there is also a need to rate the electrical influence of precipitates on the n-type Si solar cell performance. As presented in Sections 3.2.2 and 3.2.3 SiC and Si₃N₄ precipitates always show impurities leading to n-type character, which leads within p-type matrices to hetero p–n-transition. Linear (ohmic) shunting can be expected for SiC precipitates contacting the front n^+ emitter and the rear side. Regarding the case that a highly n-conducting SiC filament or cluster within the n-type silicon matrix

contacts the p^+ emitter, a tunnel contact would form to the emitter and an ohmic contact to the bulk, as for the case of Al particles [16]. This means that for n-type cells SiC filaments and also clusters should be even more harmful than for p-type cells, since here we do not need the condition that the precipitate also contacts the back contact of the cell. Modern PERC cells (p-type) with dielectric backside passivation should suffer less from material-induced shunting than conventional cells with full-area Al back contact. So the use of point contacts as the back contact of the solar cells, as mentioned in [69], also helps to reduce shunting. Theoretical band diagrams for the heterojunctions between n-SiC/p-Si and n-Si₃N₄/p-Si are shown in the Appendix.

The best way to avoid ohmic shunts caused by SiC filaments or clusters is of course to hinder the formation of them. It was reported by [35] and [36] that carbon contamination can be strongly reduced by using a melt cover not reacting with SiO vapor to CO. Alternatively, Reimann et al. [21] have reported that both SiC and Si₃N₄ precipitation can be avoided by establishing certain convective conditions not specified in detail by the authors [21]. First successes using magnetic fields are reported in [85–87]. An important approach is therefore an improved convection of the silicon melt at economical process times in order to minimize the formation of precipitates. Further adjustments to the gas management could also lead to reduced precipitate formation. A further approach to avoid non-metallic precipitates could also be in the modification or adaptation of the Si₃N₄ crucible coating in directional solidification processes, since the essential and relevant non-metallic impurity is nitrogen, either in the form of a nitrogen-correlated precipitate type or as a donor in SiC-like precipitates.

5 Conclusion During the crystallization process of silicon, especially for photovoltaic application, the enrichment of carbon and nitrogen can lead to the precipitation of the here discussed SiC and Si₃N₄ types. The different growth mechanisms as well as influences on solar cell performance of each type are discussed on basis of wide range material characterization of many scientists. The present work gives an overview of the most recent state of knowledge and is also showing some latest results.

Appendix By assuming a nitrogen doping of 6 at% within SiC precipitates with respect of the literature data shown in [73, 84], the band diagram for the heterojunction between p-Si and n-SiC can be deduced (see Fig. 12, top). Although for Si₃N₄ precipitates no linear shunting mechanism can be expected, a weak electronic activity was visible in EBIC investigations for an oxygen doped Si₃N₄ rod and the theoretical scheme of the heterojunction of these two semiconductors can be also drawn. One has to note that ΔE_B is much higher for n-Si₃N₄ compared to n-SiC and the band gap of n-Si₃N₄ is also significantly higher. But in the case of high oxygen doping also Si₃N₄ becomes n-conducting.

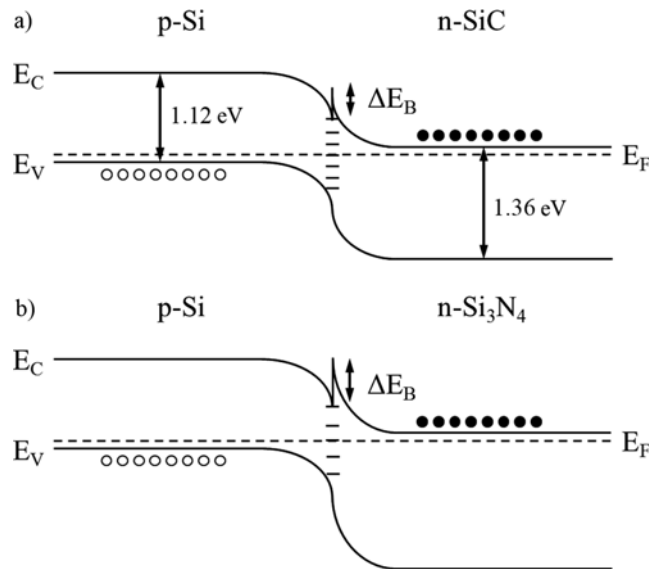


Figure 12 Schematic band diagrams of the heterojunction between p-Si and n-SiC_{1-x}N_x for $x = 0.06$ (top) and between p-Si and n-Si₃N₄ heavily doped with oxygen (bottom) (also shown in [50]).

Acknowledgements The authors are grateful for the financial support in several projects: SiThinSolar (Federal Ministry of Education and Research BMBF, contract number 03IP607), SolarFocus (Federal Ministry for the Environment, Nature Conservation and Nuclear Safety BMU, contract number 0327650D), SolarWinS (Federal Ministry for the Environment, Nature Conservation and Nuclear Safety BMU, contract number 0325270C), FzSil II (Federal Ministry of Education and Research BMBF, contract number 03SF0410F) and SolarLIFE (Federal Ministry for Economic Affairs and Energy BMWi, contract number 0325763A+D). We also thank the colleagues from Fraunhofer CSP and MPI Halle for collaboration during the last years on the field of precipitate research, namely Martina Werner, Christian Hagendorf, Angelika Hähnel, and Horst Blumtritt. We also thank Stefanie Wahl (Fraunhofer CSP) for the in this work presented ICP-MS measurements.

References

- [1] Photovoltaics Report, Fraunhofer Institute for Solar Energy Systems ISE with support of PSE AG, 6th June 2016, <https://www.ise.fraunhofer.de/de/downloads/pdf-files/aktuelles/photovoltaics-report-in-englischer-sprache.pdf>.
- [2] A. Cuevas, Multicrystalline Silicon: the photovoltaic material by excellence, Mater. Forum **27**, 1–8 (2004).
- [3] F. Schmid, P. Khattak, T. G. Digges Jr., and L. Kaufman, Origin of SiC Impurities in Silicon Crystals Grown from the Melt in Vacuum, J. Electrochem. Soc. Electrochem. Sci. Technol. **126**, 935–938 (1979).
- [4] W. Kwapil, P. Gundel, M. C. Schubert, F. D. Heinz, W. Warta, E. R. Weber, A. Goetzberger, and G. Martinez-Criado, Observation of metal precipitates at prebreakdown sites in multicrystalline silicon solar cells, Appl. Phys. Lett. **95**(23), 232113 (2009).

- [5] A. Hähnel, J. Bauer, H. Blumtritt, O. Breitenstein, D. Lausch, and W. Kwapil, Electron microscope verification of prebreakdown-inducing α -FeSi₂ needles in multicrystalline silicon solar cells, *J. Appl. Phys.* **113**, 044505 (2013).
- [6] S. Binetti, M. Acciarri, C. Savigni, A. Brianza, S. Pizzini, and A. Musinu, Effect of nitrogen contamination by crucible encapsulation on polycrystalline silicon material quality, *Mater. Sci. Eng. B* **36**(1), 68–72 (1996).
- [7] A. K. Søiland, E. J. Øvrelid, T. A. Engh, O. Lohne, J. K. Tuset, and Ø. Gjerstad, SiC and Si₃N₄ inclusions in multicrystalline silicon ingots, *Mater. Sci. Semicond. Process.* **7**, 39–43 (2004).
- [8] C. W. Lan, C. F. Yang, A. Lan, M. Yang, A. Yu, H. P. Hsu, B. Hsu, and C. Hsu, Engineering silicon crystals for photovoltaics, *Cryst. Eng. Comm.* **18**, 1474 (2016).
- [9] D. M. Chapin, C. S. Fuller, and G. L. Pearson, A new silicon p–n junction photocell for converting solar radiation into electrical power, *J. Appl. Phys.* **25**, 676–677 (1954).
- [10] A. Schönecker, L. J. Geerligs, and A. Müller, Casting Technologies for Solar Silicon Wafers: Block Casting and Ribbon-Growth-on Substrate, *Solid State Phenom.* **95–96**, 149–158 (2004).
- [11] C. V. Hari Rao, H. E. Bates, and K. V. Ravi, Electrical effects of SiC inclusions in EFG silicon ribbon solar cells, *J. Appl. Phys.* **47**, 2614–2619 (1976).
- [12] J. P. Kalejs and B. Chalmers, Melt-Interface mechanism for generation of silicon carbide microdefects in silicon, *J. Cryst. Growth* **79**, 487–492 (1986).
- [13] W. G. J. H. M. van Sark, G. W. Brandsen, M. Fleuster, and M. P. Hekkert, Analysis of the silicon market: Will thin films profit?, *Energy Policy* **35**(6), 3121–3125 (2007).
- [14] G. Bye and B. Ceccaroli, Solar grade silicon: Technology status and industrial trends, *Sol. Energy Mater. Sol. Cells* **130**, 634–646 (2014).
- [15] J. P. Rakotoniaina, S. Neve, M. Werner, and O. Breitenstein, Material-induced shunts in multicrystalline silicon solar cells, in: *Proceedings of the Conference on PV in Europe: From PV Technology to Energy Solutions*, Munich, Germany, 2002, pp. 24–27.
- [16] O. Breitenstein, J. P. Rakotoniaina, M. H. Al Rifai, and M. Werner, Shunt Types in Crystalline Silicon Solar Cells, *Prog. Photovolt.: Res. Appl.* **12**, 529–538 (2004).
- [17] M. H. Al Rifai, O. Breitenstein, J. P. Rakotoniaina, M. Werner, A. Kaminski, and N. Le Quang, Investigation of material-induced shunts in block-cast multicrystalline silicon solar cells caused by SiC precipitate filaments, in: *Proceedings of 19th European Photovoltaic Solar Energy Conference and Exhibition (EU-PVSEC)*, Paris, France, 2004, pp. 632–635.
- [18] K. Petter, Y. Ludwig, R. Bakowskie, M. Hlusiak, S. Diez, L. L. Ritz, R. Lantzsch, S. Rupp, A. Freudenberg, S. Scholz, and V. Hoffmann, Latest results on production of solar cells using UMG-Si feedstock, in: *Proceedings of 25th European Photovoltaic Solar Energy Conference and Exhibition (EU-PVSEC)*, Valencia, Spain, 2010, pp. 1624–1627, DOI: 10.4229/25thEUPVSEC2010-2CV.1.56.
- [19] M. D. Johnston, L. T. Khajavi, M. Li, S. Sokhanvaran, and M. Barati, High-Temperature Refining of Metallurgical-Grade Silicon: A Review, *JOM* **64**, 935–945 (2012).
- [20] A. K. Søiland, M. G. Dolmen, J. Heide, U. Thisted, G. Halvorsen, G. Ausland, K. Friestad, P. Preis, K. Peter, O. Graf, T. Bartel, and R. Tronstad, First results from a simplified Elkem Solar route-Input to tolerance limits, *Sol. Energy Mater. Sol. Cells* **130**, 661–667 (2014).
- [21] C. Reimann, M. Trempa, J. Friedrich, and G. Müller, About the formation and avoidance of C and N related precipitates during directional solidification of multi-crystalline silicon from contaminated feedstock, *J. Cryst. Growth* **312**, 1510–1516 (2010).
- [22] R. Zhang, E. E. Van Dyk, G. A. Rozgonyi, J. Rand, and R. Jonczyk, Investigation of foreign particles in polycrystalline silicon using infrared microscopy, *Sol. Energy Mater. Sol. Cells* **82**(4), 577–585 (2004).
- [23] V. A. Yuryev, V. P. Kalinushkin, A. P. Lytkin, and S. I. Lyapunov, Silicon-ingot inspection by active IR imaging, *Russ. Microelectron.* **33**(6), 350–352 (2004).
- [24] A. Lawrenz, M. Gosh, K. Kremmer, V. Klemm, A. Müller, and H. J. Möller, Infrared transmission investigation of rod-like defects in multicrystalline silicon, *Solid State Phenom.* **95**, 501–506 (2004).
- [25] Ø. Mjos, G. Stokkan, A. K. Søiland, and L. Arnberg, Mapping of silicon carbide and silicon nitride precipitates on chemical-mechanically polished mc-silicon wafers, in: *Proceedings of 19th European Photovoltaic Solar Energy Conference and Exhibition (EU-PVSEC)*, Paris, France, 2004, pp. 804–807.
- [26] J. P. Rakotoniaina, O. Breitenstein, M. Werner, M. H. Al-Rifai, T. Buonassisi, M. D. Pickett, M. Ghosh, A. Müller, and N. Le Quang, Distribution and formation of silicon carbide and silicon nitride precipitates in block-cast multicrystalline silicon, in: *Proceedings of 20th European Photovoltaic Solar Energy Conference and Exhibition (EU-PVSEC)*, Barcelona, Spain, 2005, pp. 773–776.
- [27] J. Bauer, O. Breitenstein, and J. P. Rakotoniaina, Precipitates and inclusions in block-cast silicon – isolation and electrical characterization, in: *Proceedings of 21st European Photovoltaic Solar Energy Conference and Exhibition (EU-PVSEC)*, Dresden, Germany, 2006, pp. 1115–1118.
- [28] J. Bauer, O. Breitenstein, and J. P. Rakotoniaina, Electronic activity of SiC precipitates in multicrystalline solar silicon, *Phys. Status Solidi A* **204**, 2190–2195 (2007).
- [29] T. Buonassisi, A. A. Istratov, M. D. Pickett, J.-P. Rakotoniaina, O. Breitenstein, M. A. Marcus, S. M. Heald, and E. R. Weber, Transition metals in photovoltaic-grade ingot-cast multicrystalline silicon: Assessing the role of impurities in silicon nitride crucible lining material, *J. Cryst. Growth* **287**, 402–407 (2006).
- [30] A. Lotnyk, J. Bauer, O. Breitenstein, and H. Blumtritt, A TEM study of SiC particles and filaments precipitated in multicrystalline Si for solar cells, *Sol. Energy Mater. Sol. Cells* **92**, 1236–1240 (2008).
- [31] S. Richter, V. Naumann, D. Lausch, M. Werner, B. März, K. Ilse, and C. Hagendorf, Trace elemental analysis of precipitates in multicrystalline silicon and investigation of solar cell shunting, in: *Proceedings of 25th European Photovoltaic Solar Energy Conference and Exhibition (EU-PVSEC)*, Valencia, Spain, 2010, pp. 1254–1258, DOI: 10.4229/25thEUPVSEC2010-2BO.3.3.
- [32] S. Richter, K. Kaufmann, and C. Hagendorf, Chemical characterization of SiC and Si₃N₄ precipitates in multicrys-

- talline silicon by NIR microscopy and ToF-SIMS, *Phys. Status Solidi C* **8**, 796–799 (2011).
- [33] P. R. Sahm, I. Egry, and T. Volkmann, Schmelze, Erstarrung, Grenzflächen: Eine Einführung in die Physik und Technologie flüssiger und fester Metalle (Springer, Berlin, 2001).
 - [34] J. Bauer, O. Breitenstein, A. Lotnyk, and H. Blumtritt, Investigations on different types of filaments in multicrystalline silicon for solar cells, in: Proceedings of 22nd European Photovoltaic Solar Energy Conference and Exhibition (EU-PVSEC), Milan, Italy, 2007, pp. 994–997.
 - [35] B. Gao, S. Nakano, and K. Kakimoto, Effect of crucible cover material on impurities of multicrystalline silicon in a unidirectional solidification furnace, *J. Cryst. Growth* **318**, 255–258 (2011).
 - [36] L. Liu, X. Qi, W. Ma, Z. Li, and Y. Zhang, Control of the gas flow in an industrial directional solidification furnace for production of high purity multicrystalline silicon ingots, *Int. J. Photoenergy* **2015**, 513639 (2015).
 - [37] A. K. Søiland, E. J. Øvrelid, O. Lohne, J. K. Tuset, T. A. Engh, and Ø. Gjerstad, Carbon and Nitrogen content and inclusion formation during crystallization of multi-crystalline silicon, in: Proceedings of 19th European Photovoltaic Solar Energy Conference and Exhibition (EU-PVSEC), Paris, France, 2004, pp. 911–914.
 - [38] M. Trempa, C. Reimann, J. Friedrich, and G. Müller, The influence of growth rate on the formation and avoidance of C and N related precipitates during directional solidification of multi crystalline silicon, *J. Cryst. Growth* **312**, 1517–1524 (2010).
 - [39] E. Scheil, Bemerkungen zur Schichtkristallbildung, *Z. Metallkunde* **34**, 70–72 (1942).
 - [40] T. Nozaki, Y. Yatsurugi, and N. Akiyama, Concentration and behavior of carbon in semiconductor silicon, *J. Electrochem. Soc.* **117**(12), 1566 (1970).
 - [41] T. Nozaki, Y. Yatsurugi, N. Akiyama, Y. Endo, and Y. Maki-de, Behaviour of light impurity elements in the production of semiconductor silicon, *J. Radioanal. Nucl. Chem.* **19**(1), 109 (1974).
 - [42] Y. Yatsurugi, N. Akiyama, Y. Endo, and T. Nozaki, Concentration, solubility, and equilibrium distribution coefficient of nitrogen and oxygen in semiconductor silicon, *J. Electrochem. Soc.* **120**(7), 975 (1973).
 - [43] P. Krishna and R. Marshall, The structure, perfection and annealing behaviour of SiC needles grown by a VLS mechanism, *J. Cryst. Growth* **9**, 319–325 (1971).
 - [44] F. Aldinger, M. Weinmann, and J. Bill, Precursor-derived Si–B–C–N ceramics, *Pure Appl. Chem.* **70**(2), 439–448 (1998).
 - [45] V. Heine, C. Cheng, and R. J. Needs, The preference of silicon carbide for growth in the metastable cubic form, *J. Am. Ceram. Soc.* **74**(10), 2630 (1991).
 - [46] J. Bauer, The Origins of Non-Ideal Current–Voltage Characteristics of Silicon Solar Cells, Dissertation Thesis, Martin-Luther-Universität Halle-Wittenberg, Germany, 2009, <http://digital.bibliothek.uni-halle.de/urn:urn:nbn:de:gbv:3:4-1951>.
 - [47] S. Köstner, A. Hähnel, R. Mokso, H. Blumtritt, and P. Werner, Structural Analysis of Longitudinal Si–C–N Precipitates in Multicrystalline Silicon, *IEEE J. Photovolt.* **3**, 566–571 (2013).
 - [48] N. Abrosimov, A. Bazhenov, and V. Tatarchenko, Growth features and local electronic properties of shaped silicon, *J. Cryst. Growth* **82**(1), 203 (1987).
 - [49] S. Richter, M. Werner, M. Schley, F. Schaaff, H. Riemann, H.-J. Rost, F. Zobel, R. Kunert, P. Dold, and C. Hagendorf, Structural and Chemical Investigations of Adopted Siemens Feed Rods for an Optimized Float Zone Process, *Energy Proc.* **38**, 604–610 (2013).
 - [50] S. Richter, Entstehung und Charakterisierung von nichtmetallischen Fremdphasen bei Siliziumkristallisationsprozessen für die Photovoltaik, Dissertation Thesis, Fraunhofer CSP and University Halle-Wittenberg, 2015, scientific report Fraunhofer CSP 6173/2015.
 - [51] H. J. Möller, C. Funke, J. Bauer, S. Köstner, H. Straube, and O. Breitenstein, Growth of Silicon Carbide Filaments in Multicrystalline Silicon for Solar Cells, *Solid State Phenom.* **156**, 35–40 (2010).
 - [52] H. J. Möller, C. Funke, D. Kreßner-Kiel, and S. Würzner, Growth optimization of multicrystalline silicon, *Energy Proc.* **3**, 2–12 (2011).
 - [53] K. Tang, E. J. Øvrelid, G. Tranell, and M. Tangstad, Thermochemical and kinetic databases for the solar cell silicon materials, in: *Crystal growth of Si for solar cells* (Springer, Berlin, 2009), pp. 219–251.
 - [54] J. Bauer, O. Breitenstein, A. Lotnyk, and H. Blumtritt, Investigations on different types of filaments in multicrystalline silicon for solar cells, in: Proceedings of the 22nd European Photovoltaic Solar Energy Conference and Exhibition (EU-PVSEC), 2007, pp. 994–997.
 - [55] J. Bauer, Charakterisierung von Siliciumkarbid- und Siliciumnitridpartikeln in blockgegossenem Silicium für Solarzellen, Diploma thesis, Max Planck Institute of Microstructure Physics and University of Halle-Wittenberg, 2006.
 - [56] S. Yoshida, Band structure of SiC: overview, in: *Properties of Silicon Carbide*, edited by G. L. Harris (INSPEC, London, 1995), p. 74.
 - [57] S. Richter, M. Werner, S. Swatek, B. März, and C. Hagendorf, Trace elemental and structural analysis of different types of Si₃N₄ precipitates grown in blockcast multicrystalline solar silicon, in: Proceedings of the 21st NREL Workshop on Crystalline Silicon Solar Cells and Modules: Materials and Processes, Breckenridge, Colorado, USA, 2011, pp. 27–34.
 - [58] N. Chen, B. Liu, S. Qiu, G. Liu, and G. Du, Study of SiC and Si₃N₄ inclusions in industrial multicrystalline silicon ingots grown by directional solidification method, *Mater. Sci. Semicond. Process.* **13**(4), 231–238 (2010).
 - [59] S. Meyer, S. Richter, and C. Hagendorf, Surface contaminations on silicon wafers – Monitoring of cleaning processes and specifying wafer quality, in: Proceedings of the Photovoltaic Specialists Conference (PVSC), 37th IEEE, 2011, pp. 001105–001107.
 - [60] T. Buonassisi, A. Istratov, M. Pickett, J.-P. Rakotoniaina, O. Breitenstein, M. Marcus, S. Heald, and E. Weber, Transition metals in photovoltaic-grade ingot-cast multicrystalline silicon: Assessing the role of impurities in silicon nitride crucible lining material, *J. Cryst. Growth* **287**(2), 402 (2006).
 - [61] V. Ganapati, S. Schönfelder, S. Castellanos, S. Öner, R. Köpge, A. Sampson, M. A. Marcus, B. Lai, H. Morhenn, G. Hahn, J. Bagdahn, and T. Buonassisi, Infrared birefrin-

- gence imaging of residual stress and bulk defects in multicrystalline silicon, *J. Appl. Phys.* **108**, 063528 (2010).
- [62] M. A. Falkenberg and M. Seibt, Transmission electron microscopy analysis of extended defects in multicrystalline silicon using in-situ EBIC/FIB sample preparation, *Phys. Status Solidi C* **10**, 32–35 (2013).
- [63] A. Krushevska, S. Tan, M. Passer, and X. R. Liu, Advances in trace element analysis of silicon wafer surfaces by vapor phase decomposition (VPD) and inductively coupled plasma mass spectrometry (ICP-MS), *J. Anal. At. Spectrom.* **15**(9), 1211 (2000).
- [64] I. E. Kononov, O. Breitenstein, and K. Iwig, Local current–voltage curves measured thermally (LIVT): A new technique of characterizing PV cells, *Sol. Energy Mater. Sol. Cells* **48**, 53–60 (1997).
- [65] O. Breitenstein, J. P. Rakotoniaina, and M. H. Al Rifai, Quantitative Evaluation of Shunts in Solar Cells by Lock-In Thermography, *Prog. Photovolt.: Res. Appl.* **11**, 515–526 (2003).
- [66] G. Hahn, D. Sontag, and C. Haessler, Current collecting channels in RGS silicon solar cells – are they useful?, *Sol. Energy Mater. Sol. Cells* **72**, 453–464 (2002).
- [67] J. P. Rakotoniaina, O. Breitenstein, M. Langenkamp, M. Werner, and G. Hahn, Investigation of 3D Inversion Channels in Solar Cells on RGS Silicon Ribbons, in: *Proceedings of 17th European Photovoltaic Solar Energy Conference and Exhibition (EU-PVSEC)*, Munich 10/2001, edited by B. McNelis, W. Palz, H. A. Ossensbrink, and P. Helm (WIP Munich and ETA-Florence, 2002), pp. 1444–1447.
- [68] H. Gottschalk, Precipitates in Ribbon Grown Solar Silicon, *Phys. Status Solidi B* **222**, 353 (2000).
- [69] O. Breitenstein, J. Bauer, and J. P. Rakotoniaina, Material-Induced Shunts in Multicrystalline Silicon Solar Cells, *Semiconductors* **41**, 440–443 (2007).
- [70] S. Köstner, H. Cypionka, H. van der Voort, J. Bauer, J.-M. Wagner, and O. Breitenstein, 3D subsurface imaging of precipitates inside block-cast silicon, in: *Proceedings of the 24th European Photovoltaic Solar Energy Conference and Exhibition (EU-PVSEC)*, Hamburg, Germany, 2009, pp. 2270–2274, DOI: 10.4229/24thEUPVSEC2009-2DV.1.83.
- [71] O. Breitenstein, J. Bauer, M. Kittler, T. Arguirov, and W. Seifert, *Scanning* **30**, 331–338 (2008).
- [72] A. Froitzheim, R. Stangl, L. Elstner, M. Kriegel, and W. Fuhs, AFORS-HET: a computer-program for the simulation of heterojunction solar cells to be distributed for public use, in: *Proceedings of the 3rd World Conference on Photovoltaic Energy Conversion*, Osaka, 2003, Vol. A, pp. 279–282.
- [73] H.-S. Liu, X.-Y. Fang, W.-L. Song, Z.-L. Hou, R. Lu, J. Yuan, and M.-S. Cao, Modification of Band Gap of β -SiC by N-Doping, *Chin. Phys. Lett.* **26**(6), 067101 (2009).
- [74] L. L. Snead, T. Nozawa, Y. Katoh, T.-S. Byun, S. Kondo, and D. A. Petti, Handbook of SiC properties for fuel performance modeling, *J. Nucl. Mater.* **371**, 329–377 (2007).
- [75] D. Chakraborty and J. Mukerji, Characterization of silicon nitride single crystals and Polycrystalline reaction sintered silicon nitride by microhardness measurements, *J. Mater. Sci.* **15**, 3051–3056 (1980).
- [76] F. Ericson, S. Johansson, and J. Å. Schweitz, Hardness and Fracture Toughness of Semiconducting Materials Studied by Indentation and Erosion Techniques, *Mater. Sci. Eng. A* **105**, 131–141 (1988).
- [77] L. J. Vandeperre, F. Giuliani, S. J. Lloyd, and W. J. Clegg, The hardness of silicon and germanium, *Acta Mater.* **55**, 6307–6315 (2007).
- [78] H. J. Möller, Basic Mechanisms and Models of Multi-Wire Sawing, *Adv. Eng. Mater.* **6**, 501–513 (2004).
- [79] G. Du, L. Zhou, P. Rossetto, and Y. Wan, Hard inclusions and their detrimental effects on the wire sawing process of multicrystalline silicon, *Sol. Energy Mater. Sol. Cells* **91**(18), 1743–1748 (2007).
- [80] G. Du, N. Chen, and P. Rossetto, Wire-sawing defects on multicrystalline-silicon wafers grown by a directional solidification method, *Semicond. Sci. Technol.* **23**, 055011 (2008).
- [81] C. Greskovich and G. E. Gazza, Hardness of dense α - and β -Si₃N₄ ceramics, *J. Mater. Sci. Lett.* **4**(2), 195–196 (1985).
- [82] S. Schönfelder, A. Sampson, V. Ganapati, R. Köpge, J. Bagdahn, and T. Buonassisi, Quantitative Stress Measurements of Bulk Microdefects in Multicrystalline Silicon, in: *Proceedings of 24th European Photovoltaic Solar Energy Conference and Exhibition (EU-PVSEC)*, Hamburg, Germany, 2009, pp. 977–980, DOI: 10.4229/24thEUPVSEC2009-2AO.3.5.
- [83] M. M’Hamdi and S. Gouttebroze, Analysis of the Residual Stress Field Associated with Particles in Multi-Crystalline Silicon, in: *Proceedings of 24th European Photovoltaic Solar Energy Conference and Exhibition (EU-PVSEC)*, Hamburg, Germany, 2009, pp. 1265–1268, DOI: 10.4229/24thEUPVSEC2009-2CV.1.39.
- [84] P. Tanner, S. Dimitrijević, and H. B. Harrison, Current mechanisms in n-SiC/p-Si heterojunctions, in: *Proceedings of Conference on Optoelectronic and Microelectronic Materials and Devices*, IEEE, 2008, pp. 41–43.
- [85] P. Dold, A. Cröll, M. Lichtensteiger, T. Kaiser, and K. Benz, Floating zone growth of silicon in magnetic fields: IV. Rotating magnetic fields, *J. Cryst. Growth* **231**(1), 95 (2001).
- [86] P. Rudolph, Travelling magnetic fields applied to bulk crystal growth from the melt: The step from basic research to industrial scale, *J. Cryst. Growth* **310**(7), 1298 (2008).
- [87] C. Kudla, A. Blumenau, F. Büllesfeld, N. Dropka, C. Frank-Rotsch, F. Kiessling, O. Klein, P. Lange, W. Miller, U. Rehse et al., Crystallization of 640 kg mc-silicon ingots under traveling magnetic field by using a heater-magnet module, *J. Cryst. Growth* **365**, 54 (2013).